Published in final edited form as:
Neuron. 2008 April 24; 58(2): 195–209. doi:10.1016/j.neuron.2008.02.017.

A Novel Presynaptic Giant Ankyrin Stabilizes the NMJ through Regulation of Presynaptic Microtubules and Trans-Synaptic Cell Adhesion

Jan Pielage, **Ling Cheng**, **Richard D. Fetter**, **Pete M. Carlton**, **John W. Sedat**, and **Graeme W. Davis**[*]

Department of Biochemistry and Biophysics, University of California, San Francisco, San Francisco, CA 94158-2822, Phone: 415-502-0529, Email: gdavis@biochem.ucsf.edu

Abstract

In a forward genetic screen for mutations that destabilize the neuromuscular junction we identified a novel long isoform of Drosophila *ankyrin2* (*ank2-L*). We demonstrate that loss of presynaptic Ank2-L not only causes synapse disassembly and retraction but also disrupts neuronal excitability and NMJ morphology. We provide genetic evidence that *ank2-L* is necessary to generate the membrane constrictions that normally separate individual synaptic boutons and is necessary to achieve the normal spacing of sub-synaptic protein domains including the normal organization of synaptic cell adhesion molecules. Mechanistically, synapse organization is correlated with a lattice-like organization of Ank2-L, visualized using extended high-resolution structured illumination microscopy. The stabilizing functions of Ank2-L can be mapped to the extended C-terminal domain that we demonstrate can directly bind and organize synaptic microtubules. We propose that a presynaptic Ank2-L lattice links synaptic membrane proteins and Spectrin to the underlying microtubule cytoskeleton to organize and stabilize the presynaptic terminal.

INTRODUCTION

The pathology of many neurodegenerative diseases involves the dying back of neuronal processes and the eventual elimination of synaptic connections. It has become apparent that synapse loss and axon retraction often precede the onset of neurodegenerative disease symptoms and generally precede neuronal death (Luo and O'Leary, 2005; Saxena and Caroni, 2007). These observations implicate synapse disassembly and axon retraction as early events in neurodegenerative disease. However, the molecular mechanisms underlying the inappropriate disassembly and retraction of synaptic connections remain poorly understood. A common observation is that synapse destabilization and axon retraction are correlated with a disruption of the underlying microtubule cytoskeleton (Pielage et al., 2005; Wang et al., 2001; Watts et al., 2003; Zhai et al., 2003). Recently it has been proposed that disruption of the neuronal microtubule cytoskeleton could even be a causal or an inductive event in disease (Wang et al., 2001). However, it remains unclear how disruption of the synaptic microtubule cytoskeleton could lead to synapse disassembly, a process that would seem to require the

*to whom correspondence should be addressed.

disruption of strong trans-synaptic protein interactions that normally stabilize synaptic connections.

Using a forward genetic approach in Drosophila we have identified mutations in a novel giant isoform of Ankyrin2 (Ank2-L) that forms a sub-membranous lattice within the presynaptic nerve terminal at the neuromuscular junction (NMJ). We demonstrate that loss of presynaptic Ank2-L results in the inappropriate destabilization and retraction of the presynaptic nerve terminal at the NMJ. Retraction of the NMJ is correlated with the disorganization of synaptic cell adhesion molecules and the disruption of the underlying microtubule cytoskeleton. We then demonstrate that the C-terminal tail of Ank2-L can directly bind and organize microtubules and is necessary for synapse stability. Based upon these and additional data, we present a model for synapse stability in which a presynaptic giant Ankryin provides a molecular link between intercellular adhesion and cytoskeletal stabilization that is necessary to maintain the integrity of the NMJ.

Ankyrins are a family of adaptor proteins that have the potential to recruit the Spectrin-based membrane skeleton to specific transmembrane proteins. Ankyrins are organized into three conserved domains: an amino terminal membrane association domain that contains 24 Ankyrin repeats organized into 4 subdomains, a Spectrin-binding domain and a C-terminal tail region that varies significantly between Ankyrins (Bennett and Baines, 2001). While canonical Ankyrins do not exceed 220 kDa, both vertebrate AnkyrinB (AnkB) and AnkyrinG (AnkG) encode giant isoforms of 440 kDa and 270/480 kDa, respectively (Chan et al., 1993; Kordeli et al., 1995). Interestingly, these giant isoforms are specifically targeted to the axon and their C-terminal tail is predicted to be up to 220 nm long and to extend deep into the axoplasm (Chan et al., 1993; Kordeli et al., 1995; Kunimoto, 1995). In contrast, AnkB isoforms that lack this C-terminal domain are restricted to the neuronal cell body (Chan et al., 1993; Kunimoto, 1995). It is hypothesized that this long C-terminal extension might be required for axonal targeting and could mediate interactions with the underlying cytoskeleton and thereby co-ordinate Ankyrin-dependent protein interactions at the cell membrane with the cell interior (Bennett and Baines, 2001). However, there is no direct evidence demonstrating that Ankyrins control the organization of the underlying cytoskeleton.

Within the vertebrate nervous system, giant Ankyrins are required for the organization and maintenance of specific membrane domains including the axon initial segment and nodes of Ranvier. AnkyrinG has been shown to bind cell adhesions molecules (e.g. L1 CAM, Nr CAM and Neurofascin), sodium channels ($Na_V1.6$), potassium channels (KCNQ) and βIV-Spectrin and is required to organize and stabilize these proteins at the axon initial segment (Jenkins and Bennett, 2001; Pan et al., 2006; Yang et al., 2007; Zhou et al., 1998). A similar mechanism of cell adhesion molecule and ion channel localization has been observed at the nodes of Ranvier (Davis et al., 1996; Jenkins and Bennett, 2002; Yang et al., 2007).

The Drosophila genome encodes two *ankyrin* genes, *ankyrin* and *ankyrin2*. The *ankyrin* gene is ubiquitously expressed and is enriched within the postsynaptic muscle membranes of the Drosophila NMJ (Dubreuil and Yu, 1994; Pielage et al., 2006). RNAi-mediated depletion of Ankyrin from the muscle does not alter the stability or function of the NMJ (Pielage et al., 2006). In contrast, expression of *ankyrin2* is restricted to the nervous system (Bouley et al., 2000; Hortsch et al., 2002). *Ankyrin2* encodes two previously annotated isoform types, a short isoform (Ank2a referred to as Ank2-S; 1159 amino acids) and long isoforms (Ank2b–e; between 2386 and 2465 amino acids). Both previously annotated isoform types share the first 1126 amino acids (aa) that contain the characteristic Ankyrin repeat domains as well as the Spectrin binding domain. These proteins differ in their unique C-terminal tail regions (Hortsch et al., 2002). Using antibodies targeted against the unique C-terminal tails it has been demonstrated that the short isoform is restricted to neuronal cell bodies while the long isoforms

(Ank2b–e) are present in axons (Hortsch et al., 2002). Initial studies provided evidence that the long isoforms (Ank2b–e) of Ank2 are required for animal viability (Hortsch et al., 2002) and that Ank2, together with the cell adhesion molecule Neuroglian, is required to suppress axonal sprouting during dendrite development (Yamamoto et al., 2006). In this study we present the first formal genetic analysis of *ank2* in Drosophila and, in so doing, identify a novel giant isoform of Ank2 (Ank2-L; 4083 aa) that is present within the presynaptic nerve terminal (Figure 1A). Based upon our data we present a model in which Ank2-L represents an important link between the membrane, the Spectrin skeleton and the underlying microtubules that is necessary for the long-term stabilization of the NMJ. We hypothesize that this function of Ank2-L could be relevant for synapse stability in vertebrate systems where Ankyrins have already been implicated in the cause of neurodegeneration.

Results

To identify genes that, when mutated, cause the inappropriate destabilization and retraction of the presynaptic nerve terminal (synaptic retraction) we have pursued a large-scale forward genetic screen based upon a previously published assay (Eaton and Davis, 2005; Eaton et al., 2002; Pielage et al., 2005). In this assay, synaptic retractions are identified by co-staining the NMJ with antibodies that label the presynaptic active zone (anti-Bruchpilot, Brp; Kittel et al., 2006; Wagh et al., 2006) and the postsynaptic membranes surrounding the presynaptic bouton (subsynaptic reticulum, SSR) (anti-Discs-large, Dlg; Budnik et al., 1996). At the wild type NMJ there is precise apposition of pre-and postsynaptic markers indicating a stable NMJ. In contrast, in mutant backgrounds that cause synapse disassembly, well organized postsynaptic Dlg staining is observed that lacks opposing presynaptic antigens. These sites within the NMJ represent retractions of the presynaptic nerve terminal (Eaton and Davis, 2005; Eaton et al., 2002; Pielage et al., 2005). This conclusion has been confirmed by ultrastructural, electrophysiological and immunohistochemical analyses using multiple pre- and postsynaptic markers (Eaton and Davis, 2005; Eaton et al., 2002; Pielage et al., 2005). Finally, use of this assay is supported by nearly identical analyses that are used to visualize the retraction and degeneration of the presynaptic motoneuron terminal at the vertebrate NMJ (Fischer et al., 2004; Fox et al., 2007; Mi et al., 2005; Pun et al., 2006).

To date we have screened approximately 2000 independent transposon induced mutations for the presence of synaptic retractions at the NMJ. In this screen we assay ~30 NMJ per mutant genotype by directly visualizing the NMJ using antibody staining with anti-Brp and anti-Dlg. Less than 0.5% of all mutations result in an increase in synaptic retractions at the NMJ compared to wild type (data not shown). Since the majority of the mutations in the screen were either semi-viable or larval lethal mutations, this result suggests that impaired animal health does not lead to an increase in synaptic retractions at the NMJ. In this screen, we identified the transposon insertion mutation *Pbac(WH)CG32373*^{f02001} that resides on left arm of chromosome 3 at position 66A10. Animals homozygous for the transposon insertion show severe synaptic retractions at more than 60% of all NMJ on muscles 6/7 (Figure 1C, F) and die at late larval/early pupal stages. The transposon *Pbac(WH)CG32373*^{f02001} is inserted within the novel annotated gene *SP2523* that resides approximately 35 kb downstream of the Drosophila *ankyrin2* (*ank2*) gene (Figure 1A; Flybase; Bouley et al., 2000; Hortsch et al., 2002).

Here we present genetic and molecular evidence that *Pbac(WH)CG32373*^{f02001} disrupts a novel, long isoform of *ank2*. This isoform corresponds to a previously uncharacterized, high molecular weight Ank2 isoform (> 400 kDa) that has was observed by western blot analysis (Hortsch et al., 2002). First, we provide genetic evidence that *Pbac(WH)CG32373*^{f02001} represents a novel allele of *ank2*. This genetic analysis involves the identification and characterization of a second transposon insertion in the *ank2* gene (*Pbac(WH)ank2*^{f00518};

referred to as *ank2*^{518}) that resides in the 6th intron of the previously annotated *ank2* gene, a site that is shared by both the short and long isoforms of *ank2* (Flybase; Bouley et al., 2000; Hortsch et al., 2002). Analysis of *ank2*^{518} homozygous mutant animals as well as animals trans-heterozygous for *ank2*^{518} and the deficiency *Df(3L)RM5-2* that completely uncovers the *ank2* locus (Hortsch et al., 2002) reveals severe synaptic retractions at 29% of the analyzed NMJs (Figure 2G). Animals of these mutant combinations die at early larval stages. Consistent with *ank2*^{518} representing a mutation in *ank2* we find that Ank2-L protein is completely absent in *ank2*^{518} and *ank2*^{518}*/Df* mutant animals (Supplemental Figure 1F). Together, these results indicate that the transposon insertion *ank2*^{518} disrupts *ank2* and that *ank2* represents an essential gene required for viability and NMJ stability.

We then tested, genetically, whether *ank2*^{518} and *Pbac(WH)CG32373*^{f02001} disrupt the same gene. We examined animals trans-heterozygous for *Pbac(WH)CG32373*^{f02001} and *ank2*^{518} and animals trans-heterozygous for *Pbac(WH)CG32373*^{f02001} and the deficiency *Df(3L)RM5-2*. Both mutant combinations die as third instar larvae/early pupae and we observe severe synaptic retractions in these animals (Figure 1D, F, G). Thus, *Pbac(WH)CG32373*^{f02001} fails to complement both the larval lethality and the synaptic retraction phenotype associated with the disruption of *ank2* by either the transposon insertion *ank2*^{518} or the deficiency *Df(3L)RM5-2*. These data are consistent with *Pbac(WH)CG32373*^{f02001} disrupting a novel long isoform of *ank2*. This conclusion is further supported by sequence analysis demonstrating the existence of a single open reading frame (*ank2-L*) that connects the last exon of the previously published long isoforms of *ank2* (*ank2b–e*) with the annotated exons of *SP2523* (Figure 1A). This open reading frame encodes a 4083 amino acid long giant Ankyrin2 (Ank2-L) with a predicted molecular weight of 449 kDa. We then verified the existence and expression of this open reading frame by RT-PCR analysis (data not shown, see Supplemental Methods).

Finally, we assayed the distribution and abundance of Ank2-L protein. In wild type animals Ank2-L is highly abundant in motoneuron axons and enriched within the presynaptic nerve terminal at the NMJ (Supplemental Figure 1A and A′). Importantly, as mentioned earlier, we cannot detect any Ank2-L protein at NMJs of *ank2*^{518}*/Df(3L)RM5-2* mutant animals indicating that the P-element insertion *ank2*^{518} disrupts the expression of *ank2-L* (Supplemental Figure 1F). In both homozygous *Pbac(WH)CG32373*^{f02001} and trans-heterozygous *Pbac(WH)CG32373*^{f02001}*/ank2*^{518} mutant animals we find that Ank2-L immunoreactivity is significantly decreased in motoneuron axons and nearly absent within the presynaptic nerve terminal (Supplemental Figure 1B, C). Together, our genetic, molecular and immunohistochemical data identify *Pbac(WH)CG32373*^{f02001} as a mutation in a novel giant isoform of Drosophila *ank2*. For simplicity, we refer to the P-element insertion *Pbac(WH)CG32373*^{f02001} *as ank2*^{2001}.

Ank2-L is required for synapse stabilization

To this point our data demonstrate that Ank2-L is required for NMJ stability. To further substantiate this conclusion, we took a second approach to specifically eliminate the Ank2-L protein from the NMJ. We generated transgenic RNAi flies that specifically target the long isoform of *ank2* (*UAS-ank2-L-RNAi*). Expression of *UAS-ank2-L-RNAi* in the nervous system leads to the partial loss of Ank2-L protein at the NMJ (Supplemental Figure 1D) and causes a significant increase in synaptic retractions (Figure 1E–G).

To further understand the requirements of *ank2-L* for synapse stability we performed a detailed analysis or the synaptic retraction phenotype in *ank2* mutant animals. First we analyzed synaptic retractions with a wide variety of pre- and postsynaptic markers. Importantly, we observe synaptic retractions at similar frequencies and with comparable severities for all cytoplasmic presynaptic markers (Brp, Synapsin (Syn), Synaptotagmin (Syt), Dap160, Nervous wreck (Nwk)) compared to postsynaptic Dlg and postsynaptic glutamate receptor

cluster staining (Figure 1, 2, Supplemental Figure 3). Through the analysis of multiple combinations of these markers we are able to propose a sequence of disassembly events during the retraction of the NMJ. The presynaptic microtubule cytoskeleton appears to be the first marker to be lost from terminal boutons. This is followed by the loss of presynaptic cytoplasmic markers (see above) and transmembrane proteins (e.g. Neuroglian (Nrg) and Fasciclin II (Fas II)). The last marker that remains in opposition to postsynaptic Dlg or glutamate receptors is the general neuronal-membrane marker HRP (Figures 2, 3 Supplemental Figures 2, 3) (for a summary see schematic in Supplemental Figure 2G and the Supplemental Discussion that follows).

An additional observation highlights the full extent of synapse retraction that we observe. We frequently observe the complete elimination of presynaptic cytoplasmic markers from NMJs that are clearly defined by organized postsynaptic Dlg staining (12 % of all NMJ on muscle 4, n = 116) (Figure 2D–F). Importantly, although the synaptic vesicle markers (Syn, Syt) and active zone markers (Brp) are completely absent, we still observe small, discontinuous remnants of the presynaptic membrane opposite organized Dlg staining (Figure 2D–F). The same phenotype can be observed when we co-stain the synapse for presynaptic microtubules (Futsch), HRP and Dlg (Supplemental Figure 2D–F). This observation supports the conclusion that the nerve terminal became fragmented as it retracted from the muscle. This is consistent with a similar process of fragmentation that occurs during axonal and dendrite retraction in other organisms (Luo and O'Leary, 2005).

Finally, it is important to emphasize that synapse retractions can also be visualized (with equivalent frequency and severity) when preparations are co-stained for presynaptic antigens and postsynaptic glutamate receptor clusters (Supplemental Figure 3E–H). Prior live imaging studies demonstrate that glutamate receptor clusters only form below the growing nerve terminal during larval development (Rasse et al., 2005). Furthermore, glutamate receptor clusters are always formed in opposition to presynaptic Brp, which is a marker that is necessary for active zone function (Kittel et al., 2006; Rasse et al., 2005; Wagh et al., 2006). Together, these data support the conclusion that a functional presynaptic nerve terminal resided in opposition to clustered glutamate receptors and subsequently retracted, leaving behind glutamate receptor clusters and remnants of the presynaptic membrane.

To address whether the destabilization and retraction of the presynaptic nerve terminal becomes phenotypically worse over time, consistent with a neurodegenerative event, we analyzed the frequency and severity of NMJ retractions throughout larval development. In the $ank2^{2001/Df}$ second instar larvae we observe synaptic retractions at only 6% of all NMJ. However, by the late 3rd instar stage (L3 late) 75% of all NMJ show signs of retractions (Figure 2H). We observe a similar, developmental increase in the severity of the synaptic retractions in these animals (Figure 2I). In addition, we show that the severity of mutations in *ank2* correlates with the severity of the retraction phenotype at a single time point (Figure 2G). In second instar larvae, *ank2* null mutations ($ank2^{518/Df}$) show retractions at 29% of all NMJ whereas the hypomorphic mutation ($ank2^{2001/Df}$) shows retractions at only 6% of the NMJs. Therefore, the synapse retractions caused by the loss of Ank2-L represent a progressive phenotype that correlates with the severity of the disruption of *ank2*.

Ank2 is necessary for the normal organization of synaptic cell adhesion molecules

Ankyrins function as adaptor molecules that organize and stabilize transmembrane proteins within specific membrane domains. A potential function of Ank2-L would be the stabilization of synaptic cell adhesion molecules. Therefore we analyzed the distribution and stability of the homophilic cell adhesion molecule Fasciclin II (Fas II) in *ank2* mutant animals. In wild type animals Fas II is organized into a honeycomb-like distribution that marks peri-active zones and the boundaries of the presynaptic nerve terminal (Figure 3A–C). In *ank2* mutant animals

we observe two distinct phenotypes. First, the organization of Fas II and HRP within the membrane is severely impaired. In contrast to wild type, both Fas II and HRP accumulate into large presynaptic aggregates (Figure 3D–F). In addition, Fas II can be severely reduced and almost absent from regions of the synapse where HRP is still present opposite postsynaptic Dlg. At the regions lacking Fas II staining, the presynaptic membrane (marked by HRP) appears fragmented implicating ongoing disassembly of the presynaptic nerve terminal at these sites (Figure 3G–H, arrow). These data are consistent with the conclusion that Ank2 is necessary for the appropriate organization and stabilization of the synaptic, homophilic cell adhesion molecule Fas II and potentially other synaptic trans-membrane proteins identified by the anti-HRP antibody staining.

Electrophysiological deficits in *ank2* mutant animals

We next tested the electrophysiological properties of neuromuscular synapses in *ank2* mutant animals. We analyzed synaptic transmission in both the second instar *ank2-L* null mutant animals ($ank^{f00518}/Df(3L)RM5\text{-}2$) as well as third instar larvae that specifically lack *ank2-L* ($ank2^{2001}/Df(3L)RM5\text{-}2$). In both cases we observe defects in synaptic transmission and motoneuron excitability consistent with a disruption of NMJ stability and consistent with a previously described function of Ankyrins to bind and organize ion channels at the plasma membrane (Supplemental Figure 4).

A presynaptic Ank2-L lattice visualized with extended high-resolution structured illumination microscopy

Ank2-L staining is observed throughout the axon and presynaptic nerve terminal at the NMJ (Supplemental Figure 1A). To visualize the organization of Ank2-L, *in vivo*, we turned to extended high-resolution structured illumination microscopy. This technique allows for 3D image acquisition with X and Y resolution approaching 100 nm (Gustafsson, 2000) and is embedded in a new generation microscope called OMX (Gustafsson et al., 2008; Carlton et al., manuscript in preparation; see methods). Synapses were co-stained for Ank2-L and Fas II and imaged using 3D-structured-illumination microscopy. Within the motoneuron axon, Ank2-L protein is closely associated with the membrane and organized into a lattice-like structure (Figure 4A). At places, repeating pentameric and hexameric structures can be observed that are reminiscent of the organization of the membrane-associated Spectrin skeleton in other tissues (Liu et al., 1987). We observe a spacing of approximately 200 nm between Ank2-L positive domains within the axon (Figure 4A, inset 1). A similar organization of β-Spectrin is observed within the axon, supporting the idea that Ank2-L is organized through binding to the submembranous Spectrin skeleton (Supplemental Figure 5).

Interestingly, the organization of Ank2-L is dramatically different within synaptic boutons (Figure 4A, B). At these sites Ank2-L is less abundant and does not show the same compact, patterned organization that is found in the axon. In addition, Ank2-L staining is found adjacent to the presynaptic active zone maker Brp and in close proximity to the synaptic cell adhesion molecule Fas II (Figure 4A, B). Finally, it appears that the constrictions that normally separate neighboring synaptic boutons contain higher levels of Ank2-L and that Ank2-L is organized in a lattice-like pattern in these regions similar to the organization observed in the axon (Figure 4B, arrows). Thus, Ank2-L shows sub-cellular differences in its organization within the presynaptic nerve terminal. These data suggest that Ank2-L, possibly through an interaction with the Spectrin skeleton, might be involved in the specification of axon, synaptic bouton and inter-bouton regions.

Several observations support the conclusion that the observed lattice of presynaptic Ank2-L is not an artifact of the structured illumination technique. First, the highly organized Ank2-L lattice bends and curves with the axon and presynaptic nerve terminal. Second, the Ank2-L

lattice shows clear organizational differences comparing the axon and synaptic boutons within a single image. Third, when a second marker is imaged at the same time as Ank2-L (such as Tubulin which is localized pre- and postsynaptically) the lattice-like pattern appears only in the Ank2-L channel. Fourth, the banding pattern is independent of the secondary antibody used to visualize Ank2-L. Fifth, we observe that anti-Brp staining is organized into a ring-like structure (Figure 4B) that is identical to that observed by STED (stimulated emission depletion) fluorescence imaging (Kittel et al., 2006). Finally, the organization of Ank2-L into a repeating pattern that includes pentagons and hexagons (~200 nm diameter) is consistent with the known organization of the Ankyrin binding protein Spectrin (Liu et al., 1987). Together, these observations give us confidence that we are visualizing the organization of Ank2-L within the presynaptic nerve terminal.

Ank2-L is required for normal presynaptic organization and morphogenesis

A detailed analysis of synapse morphology in the *ank2-L* mutants supports a role for Ank2-L in the specification of axon, synaptic bouton and inter-bouton regions as suggested by our structured illumination analysis. We observe two major changes in the morphology of the NMJ in *ank2-L* mutant animals. First, in wild type animals the NMJ is organized into a series of synaptic boutons that can be visualized by the membrane marker HRP and the synaptic vesicle associated protein Synapsin (Syn) (Figure 5A). In contrast, in $ank^{518/Df}$ null mutant animals (L2) the presynaptic nerve terminal lacks discrete evenly spaced synaptic boutons and characteristic narrow diameter inter-bouton regions are almost completely absent (Figure 5B, asterisk). Second, we observe enlarged membrane compartments, containing synaptic antigens such as Syn and Brp, that would normally encompass several individual synaptic boutons (Figure 5B, D). Quantification of these phenotypes in mutant third instar $ank2^{2001/Df}$ animals reveals enlarged synaptic compartments at 42% of the NMJs and altered presynaptic membrane morphology at 94% of the NMJs on muscle 4 (segments A2–A5; n = 116). The enlarged synaptic compartments at third instar synapses do not always encompass the entire NMJ, but can be observed to affect the majority of boutons at an NMJ (e.g. Figure 3D, Supplemental Figure 1B, C). This is a highly penetrant and unusual perturbation of presynaptic morphology that is never observed in wild type. These severe morphological phenotypes are already observed at the second instar NMJ at a time when NMJ retractions are just becoming prevalent. Thus, the synapse morphology phenotypes are either evidence of altered synapse development, or are representative of an early stage in the NMJ retraction process.

Ank2-L is required for normal presynaptic microtubule organization

In wild type animals the presynaptic microtubule cytoskeleton is organized into a narrow core filament that extends throughout the entire presynaptic terminal (Figure 6A, C; Roos et al., 2000). One characteristic is that the core microtubule filament, visualized by antibodies directed against the microtubule-associated protein Futsch, becomes progressively thinner as it extends into the most distal regions of the presynaptic nerve terminal (Figure 6A, C; Roos et al., 2000). In *ank2* mutant animals the presynaptic microtubule cytoskeleton is severely disorganized. In *ank2-L* null mutant second instar synapses ($ank2^{518/Df}$) we observe regions that contain disorganized accumulations of Futsch staining (Figure 6B, asterisks) and regions that are almost completely devoid of presynaptic Futsch staining (Figure 6B, arrow). Similar phenotypes are observed in third instar hypomorphic *ank2-L* mutant animals ($ank2^{2001/Df}$; Figure 6D). The quantification of these phenotypes reveals large accumulations of Futsch, that fill at least one entire bouton, in 60% of all NMJ on muscle four (segments A2–A5; n = 99). In addition, 31% of the synapses contain only very thin Futsch filaments or Futsch staining is completely absent from these NMJ (e.g. Supplemental Figure 2D–F). Therefore, at more than 90% of the NMJs on muscle 4 we find an aberrant organization of the presynaptic microtubule cytoskeleton. To ensure that the disorganized Futsch staining accurately represents a disorganization of the underlying presynaptic microtubule cytoskeleton we directly imaged

microtubules and Futsch using structured illumination microscopy. In wild type animals the high-resolution imaging reveals a close association of Futsch and microtubules within the presynaptic nerve terminal (Figure 6E, insets). In *ank2*^{2001}/*Df(3L)RM5-2* mutant animals we find that aberrant accumulations of Futsch correspond to aberrant accumulations of the underlying microtubule cytoskeleton (Figure 6F, insets). These data demonstrate that *ank2-L* is required for the organization and, possibly, the stabilization of the presynaptic microtubule cytoskeleton.

Ultrastructural analysis confirms the presence of active zones within abnormal presynaptic compartments

We next pursued an ultrastructural analysis of *ank2-L* mutant synapses (*ank2*$^{2001/Df}$) to address several questions raised by our light level analysis. EM analysis was performed at muscles 6/7 where we find all characteristics of synapse disassembly and altered synapse morphology at the light level (Figures 1, 3, Supplemental Figure 3). At the ultrastructural level, we observe NMJs that show hallmarks of NMJ retraction and disassembly including accumulations of endosomal/vacuole-like membrane profiles (Figure 7C, D). We also find regions where small presynaptic membrane profiles exist within large regions of postsynaptic SSR membrane that are less compact and less well organized compared to wild type (data not shown). These features are nearly identical to those documented in regions of synapse retraction in *dynein/dynactin* mutations and *spectrin*^{RNAi} animals (Eaton et al., 2002; Pielage et al., 2005). In addition, we observe severely enlarged presynaptic areas within the NMJ (Figure 7E, F) that correspond to the enlarged presynaptic membrane compartments that we observe at the light level (Figures 5D, 6 D, F). In these enlarged presynaptic compartments we find clearly defined pre- and postsynaptic densities (electron dense structures) and associated vesicle clusters (Figure 7E, F). It is interesting to note that active zones are often curved in cross section whereas, in wild type, active zones nearly always conform to a flat plane (compare Figure 7A to E and F). Finally, within these regions we also find large accumulations of presynaptic microtubules that form characteristic zones of exclusion lacking synaptic vesicles (Figure 7F, asterisks). Similar profiles were never observed in wild type (n > 100 boutons). These ultrastructural data support our light level observations indicating that Ank2-L is required to define the normal shape and dimension of presynaptic boutons, and that Ank2-L is required for the normal organization of the presynaptic microtubule cytoskeleton.

The unique C-terminus of Ank2-L contains a microtubule-binding domain and alters the organization and stability of microtubules in S2 cells

The C-terminal tails of giant Ankyrins have been implicated in the axonal trafficking of Ankyrins and, because they can potentially extend into the cytosol, could interact with proteins at significant distances (~220 nm) from the plasma membrane (Bennett and Baines, 2001; Chan et al., 1993; Kunimoto, 1995). The long C-terminal domain of Ank2-L contains repeat stretches of highly charged amino acids that could potentially interact with microtubules. To test this possibility we generated two N-terminal YFP-tagged constructs that include either a portion of the C-terminus (YFP-Ank2-L4; amino acids 1530–3005) or almost the entire C-terminus that is unique to Ank2-L (YFP-Ank2-L8; amino acids 1530–4083). To distinguish between protein properties unique to the C-terminal and those common to all isoforms of *ank2* we also generated an N-terminal YFP-tagged construct that includes the entire open reading frame of the short isoform of *ank2* (YFP-Ank2-S; amino acids 1–1159) (Figure 8A). The expression of the C-terminal YFP-tagged domains (YFP-Ank2-L4 or YFP-Ank2-L8) in Drosophila S2 cells results in a dramatic transformation of the microtubule cytoskeleton (Figure 8B, right panels). In contrast to untransfected cells (Figure 8B, asterisk) we observe a significant increase in microtubule abundance and a dramatic change in microtubule organization. The transfected cells lose their normal round shape and develop long spike-like processes that contain microtubule filaments (Figure 8B, arrows). Importantly, the YFP signal

always co-localizes with the altered microtubule cytoskeleton (Figure 8B, arrows). In contrast, transfection of Drosophila S2 cells with the YFP-Ank2-S construct did not alter microtubule organization or abundance (Figure 8B, left panels). These data demonstrate that the C-terminal tail of Ank2-L can co-localize and strongly influence the organization and, possibly, stabilization of microtubules in S2 cells.

To further examine the potential microtubule binding characteristics of Ank2-L we performed a microtubule pelleting assay *in vitro*. For these experiments we focused on the region within the C-terminal tail that contains repeats of charged amino acids predicted to be able to interact with microtubules. We expressed a recombinant protein that contains the amino acid residues 1682–2089 of Ank2-L fused to a His_6-tag. The purified protein was incubated with taxol-stabilized microtubules and then pelleted by centrifugation through a glycerol cushion. The His_6-$Ank2^{1682–2089}$ protein can only be detected in the pellet in the presence of taxol-stabilized microtubules indicating that this domain of Ank2-L can directly bind to microtubules (Figure 8C). Together with our S2-cell data this demonstrates that Ank2-L can directly bind to and efficiently alter the organization and stability of microtubules.

The C-terminus of Ank2-L is necessary and sufficient for synaptic targeting

We next assayed whether the C-terminal tail of Ank2-L might function similarly *in vivo* at the NMJ. In support of a direct interaction between Ank2-L and the presynaptic microtubule cytoskeleton, we find a close association between Ank2-L and the Futsch-positive presynaptic microtubule cytoskeleton in wild type animals (Supplemental Figure 6). We generated transgenic flies that allow the tissue specific expression of the three YFP-tagged Ank2 constructs (YFP-Ank2-L4, YFP-Ank2-L8 and YFP-Ank2-S). When we express YFP-Ank2-L4 or YFP-Ank2-L8 in the presynaptic motoneuron we observe efficient trafficking of the YFP-tagged proteins into the presynaptic nerve terminal (Figure 8D, right panel and data not shown). In contrast, the YFP-Ank2-S protein does not traffic to the NMJ (Figure 8D, left panel). As a control, we demonstrate that YFP-Ank2-S expression in muscle leads to trafficking of YFP-Ank2-S protein to the muscle membrane and the postsynaptic SSR membrane in a pattern similar to endogenous muscle Ankyrin, indicating that this transgene encodes a functional protein (Supplemental Figure 7A, B) (Pielage et al., 2006). Together, these data demonstrate that the unique C-terminus of Ank2-L is both necessary and sufficient for the presynaptic trafficking of Ank2-L protein in neurons.

These transgenes enabled us to test whether we could partially rescue the synaptic retraction or the morphology phenotype by expressing either the short isoform of Ank2 (YFP-Ank2-S) or only the C-terminal tail domain of Ank2-L (YFP-Ank2-L8) in $ank2^{2001/Df}$ mutant animals. We do not observe a significant rescue of either the synapse stability phenotype (53% NMJs with retractions with YFP-Ank2-L8, n = 120; 65% NMJs with retractions with YFP-Ank2-S, n = 100) or the microtubule accumulation phenotype (53% NMJs contain Futsch accumulations in the presence of YFP-Ank2-L8, n = 83). This indicates that the entire Ank2-L protein containing the membrane association domain, the Spectrin binding domain and the C-terminal microtubule-binding domain is required for normal synapse formation and stability.

Finally, we analyzed the phenotypic consequences of presynaptic over-expression of the C-terminal tail of Ank2-L in wild type animals. When we express high levels of YFP-Ank2-L8 in motoneurons, synapse morphology is severely perturbed (Figure 8E, right panel). The NMJ becomes highly ramified with the appearance of small boutons that project off the main shaft of the NMJ, similar to previously described ‘satellite boutons’ (Coyle et al., 2004; Dickman et al., 2006; Marie et al., 2004; Sweeney and Davis, 2002). The satellite boutons can be visualized by anti-HRP staining as well as by staining for the synaptic vesicle protein Synapsin (Figure 8E, right panel). Interestingly, even within single, small satellite boutons, Synapsin staining is partitioned into discrete domains similar to that observed in normally sized wild

type boutons (Figure 8E, compare left and right panels, arrow). The microtubule cytoskeleton visualized with anti-Futsch remains well organized, and small Futsch-positive filaments extend into satellite boutons (data not shown). These data demonstrate that the C-terminus of Ank2-L is sufficient to alter NMJ morphology. The presence of highly ramified, small synaptic boutons is quite different from the enlarged boutons observed in the loss of function mutations. These data are consistent with the C-terminal domain having activity (gain-of-function or neomorphic) during NMJ development that is independent of the membrane-binding and Spectrin-interacting domains of Ank2-L. We hypothesize that this activity is related to the microtubule binding activity of the Ank2-L C-terminal domain at the NMJ.

DISCUSSION

In a forward genetic screen for mutations that cause synapse retraction at the Drosophila NMJ we identified a mutation that specifically disrupts a novel long isoform of the Drosophila *ankyrin2* gene. We present genetic, immunohistochemical, molecular and biochemical evidence for the existence of a novel giant, 449 kDa Ankyrin2 (Ank2-L) isoform. This isoform forms a lattice-like structure that is concentrated within the axon and presynaptic nerve terminal. We then demonstrate, using both gene specific RNAi and multiple independent *ank2* mutations, that Ank2-L has two prominent functions at the NMJ. The loss of Ank2-L causes a progressive phenotype of synapse retraction and, ultimately, synapse elimination demonstrating that this presynaptic giant Ankyrin is necessary for synapse stability. Loss of Ank2-L also causes the loss of normal synaptic bouton shape, implicating the highly organized presynaptic Ank2-L lattice as a fundamental component that controls synaptic morphology.

Although the *ank2* gene encodes both short and long isoforms, several lines of evidence indicate that the stabilizing function of Ank2 is contributed primarily by the giant, presynaptic *ank2-L* isoform. First, the $ank2^{2001}$ transposon insertion specifically disrupts the *ank2-L* open reading frame and causes synapse retraction. Second, RNAi-mediated knock down of the *ank2-L* isoform causes synapse retraction. Third, the short isoform of *ank2* is not sufficient to rescue synapse stability in the *ank2* mutant background. Thus, while we cannot formally rule out participation of the Ank2 short isoform at some level, our data support the conclusion that loss of Ank2-L is the primary cause of presynaptic retraction and degeneration.

Giant Ankyrins and the Mechanisms of Neurodegenerative Disease

In the vertebrate nervous system, mutations in giant Ankyrins have been associated with neurodegeneration. For example, the cerebellar specific knockout of *ankG* causes progressive ataxia and loss of Purkinje cells (Zhou et al., 1998). In *ankB* knockout mice, hypoplasia of corpus collosum and pyramidal tracts and a degeneration of the optic nerve have been observed (Scotland et al., 1998). While AnkB is not required for the formation of optic nerve connections, significant neurodegeneration is observed by postnatal day 9 in *ankB* mutant animals and by postnatal day 20 nearly complete degeneration of the optic nerve can be observed (Scotland et al., 1998). AnkB is required for the maintenance of the axonal localization of the cell adhesion molecule L1-CAM, and the loss of L1-CAM precedes axon degeneration in the knockout mice (Scotland et al., 1998). Although these important studies establish a causal link between giant Ankyrins and neurodegeneration, it is unknown whether synapse loss precedes neurodegeneration in *ankB* or *ankG* knockout mice. Mechanistically, it also remains unknown which essential cellular functions of *ankB* or *ankG* are particularly relevant to the initiation or progression of neurodegeneration.

It is well established that the disruption of the axonal or synaptic microtubule cytoskeleton is an early event that is correlated with the induction and initial phases of neurodegeneration (Wang et al., 2001; Zhai et al., 2003). Here we demonstrate that synapse retraction following loss of Ank2-L is correlated with a severe disruption and eventual elimination of the synaptic

microtubule cytoskeleton, documented at both the light and EM levels. Several experiments suggest that Ank2-L directly controls synaptic microtubule organization and stability. First, presynaptic Ank2-L resides in close proximity to synaptic microtubules, as visualized by extended high-resolution structured illumination microscopy. Second, we find that a region within the C-terminal tail of Ank2-L binds microtubules *in vitro*. Third, the C-terminal microtubule-binding region of Ank2-L is sufficient to re-organize the microtubule cytoskeleton in S2 cells, resulting in aberrant microtubule bundling and increased Tubulin levels. However, expression of only the C-terminus of Ank2-L is not sufficient to rescue microtubule organization or synapse stability in *ank2* mutant animals. Therefore, although Ank2-L is able to bind microtubules, we hypothesize that the organization and stabilization of synaptic microtubules depends equally upon the association of Ank2-L with either the sub-membranous Spectrin-actin skeleton and/or with synaptic cell adhesion molecules. Evidence in favor of the involvement of synaptic cell adhesion molecules is the observation that Fas II (and Nrg) staining becomes severely disorganized and unstable in *ank2-L* mutant NMJs. In addition, we demonstrate that Ank2-L resides in close proximity to Fas II within synaptic boutons. Importantly, it has been previously demonstrated that, in *fasII* null mutant animals, the NMJ can form normally but then retracts over time (Schuster et al., 1996). Interestingly, the phenotype of complete NMJ elimination observed in these prior studies is quantitatively similar to what we observe here (e.g. complete eliminations at 5% of the NMJ on muscle 3 in *fasII* null mutant mosaic animals; Schuster et al., 1996). Since Fas II is necessary for synapse stability, it seems reasonable to propose that the loss of Fas II protein in the *ank2* mutants contributes to the loss of NMJ stability and subsequent NMJ retraction. It has previously been speculated that the large intracellular tail of giant Ankyrins could extend significant distances (220 nm) within the cell cytoplasm (Bennett and Baines, 2001). Taking this into account, Ank2-L is ideally suited to function as a stabilizing bridge between cell adhesion molecules at the synaptic plasma membrane and the underlying synaptic microtubule cytoskeleton. We hypothesize, therefore, that the loss of this molecular link between microtubules and cell adhesion is the primary cause of synapse destabilization in Drosophila *ank2* mutations.

A highly organized presynaptic Ank2-L lattice may define synaptic bouton shape

Here we have visualized the organization of a giant Ankyrin within the axon and presynaptic nerve terminal by taking advantage of the increased resolution of structured illumination microscopy (Gustafsson, 2000; Gustafsson et al., 2008). Our data are consistent with the presence of a highly organized Ank2-L lattice throughout the axon. Remarkably, the lattice-like organization of Ank2-L is modified within specific subdomains of the presynaptic nerve terminal. Ank2-L has a tight, lattice-like organization between synaptic boutons, but a less regular, sparsely connected organization within synaptic boutons. The modulation of Ank2-L organization may have functional significance for NMJ development and stabilization. Synaptic bouton organization is severely perturbed in *ank2-L* mutant animals including the loss of narrow-diameter, inter-bouton regions. The majority of the NMJ appears as a presynaptic ribbon of uniform width rather than the characteristic “beads on a string” type organization. This phenotype suggest that the Ank2-L lattice may be involved in either the developmental partitioning the presynaptic nerve terminal into distinct synaptic bouton and inter-bouton regions, or the maintenance of these discrete domains over time. This phenotype is remarkable when one considers that the majority of identified Drosophila mutations affect either the number and size of synaptic boutons, or the branching pattern of boutons on the muscle surface, but do not prevent the neuron from generating the membrane expansions that will eventually become synaptic boutons e.g. (Aberle et al., 2002; Roos et al., 2000)

The mechanisms that differentiate presynaptic boutons from axons, whether one considers *en passent* boutons or boutons that form at the end of an axon, are fundamental to the organization and function of the nervous system. One model, based upon our data, is that the highly

organized Ank2-L lattice provides the structural integrity necessary to maintain a tight tubular shape for the axon and inter-bouton regions. Bouton formation might then be associated with the regulated relaxation of the Ank2-L lattice, which could allow for the expansion of the presynaptic membrane into a synaptic bouton. It is likely that the Ank2-L lattice is coincident with a similar organization of the presynaptic Spectrin skeleton. Indeed β-Spectrin staining shows a similar organization in the axon like Ank2-L with an approximate ~200 nm repeat structure and evidence of pentameric and hexameric structures (Supplemental Figure 5). Thus, our model remains consistent with the well-established function of the Spectrin skeleton in maintaining cell shape (Bennett and Baines, 2001).

The C-terminal domain of Ank2-L is necessary and sufficient for synaptic localization

In vertebrates, expression of giant Ankyrins is restricted to the nervous system and these proteins are targeted to the axon. Interestingly, short Ankyrin isoforms, encoded by the same genes, are restricted to the cell body suggesting that the C-terminal domain is required for axonal targeting (Chan et al., 1993; Kordeli et al., 1995; Kunimoto, 1995). The mechanisms that control the trafficking and localization of giant Ankyrins to discrete locations within a neuron are fundamentally important for ion channel and cell adhesion molecule organization at the nodes of Ranvier and the axon initial segment (Ango et al., 2004; Boiko et al., 2007; Jenkins and Bennett, 2001; Pan et al., 2006; Zhou et al., 1998) and, as shown here, both synapse morphology and stabilization. However, the detailed mechanisms that regulate the trafficking and localization of giant Ankyrins within a neuron are generally unknown. A structure-function analysis of the 270 kDa giant AnkG demonstrated that multiple domains, including the membrane-binding, Spectrin-binding and a serine-rich region within the C-terminal tail, cooperate in targeting and restriction of AnkG to specific axonal domains within dorsal root ganglion neurons (Zhang and Bennett, 1998). In Drosophila, the short and long isoforms of Ank2 localize to different neuronal compartments. Similar to vertebrate AnkB (Chan et al., 1993), the short isoform is restricted to the cell body while the long isoform is found in axons (Hortsch et al., 2002) and the presynaptic nerve terminal (Figure 4A, B). We have identified a domain within the novel C-terminal extension of Ank2-L that is necessary and sufficient for trafficking Ank2-L to the axon and presynaptic nerve terminal. Presumably, the mechanisms of microtubule binding and axonal trafficking will be separable functions that map to discrete sequences within the C-terminus of Ank2-L.

MATERIALS AND METHODS

Fly stocks

Flies were maintained at 25°C on normal food. The following strains were used in this study: w^{1118} (wild type), *Pbac(WH)CG32373*^{f02001} (P(*CG32373*^{2001}) or *ank2*^{2001}), *Pbac(WH) ank2*^{f00518} (*ank2*^{518}) (both mutations were identified in the BDGP/Exelixis gene disruption project), Df(3L)RM5–2 (all from the Bloomington stock center, Indiana), *BG57*-Gal4 (Budnik et al., 1996), *elav*^{C155}-Gal4, *sca*-Gal4, UAS-*α-spectrin*-dsRNA and UAS-*β-spectrin*-dsRNA (Pielage et al., 2005). The transposon insertion collection for the screen was obtained form the Bloomington stock center, Indiana.

Generation of the *ank2* Constructs and Germline Transformation

We used the pWIZ-Vector (Lee and Carthew, 2003) to generate the UAS-*ank2-L*-dsRNA construct. The target sequence was selected to avoid significant homology with any other Drosophila gene to ensure specificity of the resulting dsRNA. We introduced *Xba*I restriction sites (underlined) to allow direct cloning into the pWIZ vector (Lee and Carthew, 2003). The following primers were used to amplify a 580 bp fragment of the *ankyrin2* open reading frame starting at position 4397 relative to the start codon of the *ankyrin2* cDNA: 5′-GGGCGGGTTCTAGAAGGTTGAAAACATTATTAGCTCC and 5′-

GGGCGGGTTCTAGAGCTGCTCATCGCCCAGTCCGGCG. The DNA-fragment was amplified from wild type genomic DNA and cloned into pWIZ according to Lee and Carthew, 2003. The UAS-*YFP-ank2-S* construct was generated by amplifying the entire *ank2-S* open reading frame from the RH63474 cDNA and direct cloning into the UAS-N-terminal Venus (EYFP) vector (T. Murphy, Drosophila Genomics Resource Center, Indiana) using the Gateway-cloning system (Invitrogen). The following primers were used to amplify the *ank2-S* open reading frame: 5′-CACCATGGTCACCGAAAATGGAG and 5′- TTACCAAATGAGCGAGAAGC. The YFP (Venus)-tagged C-terminal *ank2-L* constructs were generated by amplifying a 4428 bp long fragment for UAS-*YFP-ank2-L4* and a 7665 bp long fragment for UAS-*YFP-ank2-L8* from a mixed-staged embryonic cDNA library and cloning into the UAS-N-terminal Venus vector. The following primers were used: ank2-L4 5′- CACCCGAATCCAGCAAATTAACGAA and 5′-GATGTCTCGGTTTTAAGTCG; ank2-L8 5′- CACCCGAATCCAGCAAATTAACGAA and 5′-TTAGTGGCCCTGCTGTGG. The His_6-tagged ank2-L(1682–2089) construct was generated by PCR and cloned into a Gateway N-terminal His_6 vector. The following primers were used: ank2-His_6 5′- CACCGTCCAGGACATTAGTGCT and ank2- His_6 5′-TTAGTTTTGTTGCTCCATGCTCA. The All constructs were confirmed by sequencing. Transgenic flies were generated by standard methods. At least two independent transgene insertions were established on chromosomes 2 and 3.

Immunocytochemistry

Wandering third instar larvae were dissected in HL3 saline and fixed either with 4% Paraformaldehyde/PBS for 15 min or in Bouin's fixative (Sigma) for 1–2 minutes. Primary antibodies were applied at 4°C overnight. Primary antibodies were used at the following dilutions: anti-Bruchpilot (nc82) 1:100; anti-Fasciclin II (1D4) 1:10; anti-Synapsin 1:10; anti-Futsch (22C10) 1:50 (all provided by the Developmental Studies Hybridoma Bank, Iowa); rabbit anti-Dlg 1:5.000 (gift from V. Budnik); mouse anti-Ankyrin2-S 1:500; rat anti-Ankyrin2-L 1:500 (both gifts from M. Hortsch); rabbit anti-Dap160 1:200; mouse anti-Tubulin 1:500; mouse anti-GFP 1:500 (Molecular Probes). All secondary antibodies and Cy3 and Cy5 conjugated anti-HRP were obtained from Jackson Immunoresearch Laboratories and Molecular Probes and used at a 1:200 to 1:1000 dilution and applied for 1–2 hours at room temperature (RT). Larval preparations were mounted in Vectashield (Vector). Drosophila S2 cells were transfected with the different UAS-*YFP-ank2* constructs according to the manufacturer's manual (Invitrogen). Cells were fixed in ice-cold methanol for 5 min and stained with mouse anti-Tubulin 1:500 and an Alexa-555-labeled secondary antibody. Images were captured at room temperature using an Axiovert 200 (Zeiss) inverted microscope, a 100 × Plan Apochromat objective (Aperture 1.4) and a cooled CCD camera (Coolsnap HQ, Roper). Intelligent Imaging Innovations (3I) software was used to capture, process and analyze images.

Microtubule Binding Assay

The His_6-tagged $Ank2^{1682–2089}$ fusion protein was purified with the B-PER 6xHis fusion protein spin purification kit (Pierce) according to the manufacturer's protocol. Microtubule pelleting assays were performed using the Microtubule binding protein spin-down assay kit (Cytoskeleton, Inc.) according to the manufacturer's protocol with slight modifications. In brief, taxol stabilized microtubules were mixed with 10 μg recombinant protein and layered on top of a 60% glycerol cushion buffer. Microtubules were pelleted by centrifugation at 39,000 rpm for 10 min in a TLA-100 rotor (Beckman Coulter). After centrifugation, pellets and supernatants were collected for SDS-PAGE analysis.

Structured Illumination Microscopy

High-resolution images were obtained with a custom-built microscope ("OMX"), which incorporates a recently developed imaging technique called three-dimensional structured

illumination microscopy, or 3dSIM (Gustafsson et al., 2008). In 3dSIM, samples of interest are illuminated with a striped pattern of light, rather than uniform illumination. The stripe pattern has the effect of encoding fine details into the observed images in the form of interference fringes, in the same manner as the formation of Moiré fringes by macroscopic objects such as two mesh screens. In frequency space (after a Fourier transform), the raw image of a sample under 3dSIM consists of the sum of five copies of image data, each of which have been shifted towards the origin (toward lower spatial frequencies) by a known amount. The goal of 3dSIM imaging is to separate the five copies and shift them back to their proper location in frequency space, creating an image with twice the resolution. To generate a stripe pattern, laser light was passed through a diffraction grating, and the three central diffraction orders (−1, 0, and +1) are brought to focus in the back focal plane of the microscope objective. These beams then interfere with each other in the sample plane, causing a three-dimensional interference pattern. In order to obtain sufficient information to separate out the individual components encoded in the interference pattern, the grating was rotated and translated to provide three orientations and five phases of the stripe pattern. After separation, the five frequency-space components can then be moved to their proper positions where they specify fine details. The reconstructed frequency space images were then inverse Fourier transformed, resulting in images with double the resolution compared to conventional wide field images; specifically, the X and Y resolution approaches 100nm. Images were acquired with a spacing in Z of 0.125μm; one Z stack was acquired at each orientation of the diffraction grating, for a total of three Z stacks. This microscope will be commercially available through Applied Precision, Washington.

Electrophysiology

Third instar larvae were selected and dissected according to previously published techniques (Pielage et al., 2005). Whole muscle recordings were performed on muscle 6 in abdominal segment A3 using sharp microelectrodes (12–16MΩ) according to previously published methods (Pielage et al., 2005).

Electron microscopy

Third instar larvae, mutant and wild type, were prepared for electron microscopy as follows. Larvae were filleted and pinned out in physiological saline that was then exchanged with 2% glutaraldehyde in 0.12M Na-cacodylate buffer, pH 7.4. The filleted larvae were fixed in place for 10 minutes, then transferred to vials containing fresh fixative and fixed for a total of 2 hours with rotation. The larvae were rinsed with 0.12M Na-cacodylate buffer, and postfixed with 1% osmium tetroxide in 0.12M Na-cacodylate buffer for 1 hour. Following post fixation, the specimens were rinsed with 0.12M Na-cacodylate buffer, followed by water, and then stained *en bloc* with 1% aqueous uranyl acetate for 1 hour. The larvae were rinsed with water, dehydrated and embedded in Eponate 12 resin. Sections were cut with a Leica Ultracut E microtome, collected on Pioloform coated slot grids, and stained with uranyl acetate and Sato's lead. Sections were photographed with a Tecnai spirit operated at 120 kV equipped with a Gatan 4k × 4k camera.

Supplementary Material

Refer to Web version on PubMed Central for supplementary material.

Acknowledgments

We would like to thank V. Budnik, Michael Hortsch and the Developmental Studies Hybridoma Bank, Iowa for antibodies, the Drosophila Genomics Resource Center for reagents and R. Carthew for the pWIZ vector. We thank Dion Dickman for critical reading of a prior version of this manuscript. This work was supported by a fellowship of the Deutsche Forschungsgemeinschaft to J. Pielage and National Institutes of Health grant NS047342 to G.W. Davis.

References

Aberle H, Haghighi AP, Fetter RD, McCabe BD, Magalhaes TR, Goodman CS. wishful thinking encodes a BMP type II receptor that regulates synaptic growth in Drosophila. Neuron 2002;33:545–558. [PubMed: 11856529]

Ango F, di Cristo G, Higashiyama H, Bennett V, Wu P, Huang ZJ. Ankyrin-based subcellular gradient of neurofascin, an immunoglobulin family protein, directs GABAergic innervation at purkinje axon initial segment. Cell 2004;119:257–272. [PubMed: 15479642]

Bennett V, Baines AJ. Spectrin and ankyrin-based pathways: metazoan inventions for integrating cells into tissues. Physiol Rev 2001;81:1353–1392. [PubMed: 11427698]

Boiko T, Vakulenko M, Ewers H, Yap CC, Norden C, Winckler B. Ankyrin-dependent and -independent mechanisms orchestrate axonal compartmentalization of L1 family members neurofascin and L1/neuron-glia cell adhesion molecule. J Neurosci 2007;27:590–603. [PubMed: 17234591]

Bouley M, Tian MZ, Paisley K, Shen YC, Malhotra JD, Hortsch M. The L1-type cell adhesion molecule neuroglian influences the stability of neural ankyrin in the Drosophila embryo but not its axonal localization. J Neurosci 2000;20:4515–4523. [PubMed: 10844021]

Budnik V, Koh YH, Guan B, Hartmann B, Hough C, Woods D, Gorczyca M. Regulation of synapse structure and function by the Drosophila tumor suppressor gene dlg. Neuron 1996;17:627–640. [PubMed: 8893021]

Chan W, Kordeli E, Bennett V. 440-kD ankyrinB: structure of the major developmentally regulated domain and selective localization in unmyelinated axons. J Cell Biol 1993;123:1463–1473. [PubMed: 8253844]

Coyle IP, Koh YH, Lee WC, Slind J, Fergestad T, Littleton JT, Ganetzky B. Nervous wreck, an SH3 adaptor protein that interacts with Wsp, regulates synaptic growth in Drosophila. Neuron 2004;41:521–534. [PubMed: 14980202]

Davis JQ, Lambert S, Bennett V. Molecular composition of the node of Ranvier: identification of ankyrin-binding cell adhesion molecules neurofascin (mucin+/third FNIII domain) and NrCAM at nodal axon segments. J Cell Biol 1996;135:1355–1367. [PubMed: 8947556]

Dickman DK, Lu Z, Meinertzhagen IA, Schwarz TL. Altered synaptic development and active zone spacing in endocytosis mutants. Curr Biol 2006;16:591–598. [PubMed: 16546084]

Dubreuil RR, Yu J. Ankyrin and beta-spectrin accumulate independently of alpha-spectrin in Drosophila. Proc Natl Acad Sci U S A 1994;91:10285–10289. [PubMed: 7937942]

Eaton BA, Davis GW. LIM Kinase1 controls synaptic stability downstream of the type II BMP receptor. Neuron 2005;47:695–708. [PubMed: 16129399]

Eaton BA, Fetter RD, Davis GW. Dynactin is necessary for synapse stabilization. Neuron 2002;34:729–741. [PubMed: 12062020]

Fischer LR, Culver DG, Tennant P, Davis AA, Wang M, Castellano-Sanchez A, Khan J, Polak MA, Glass JD. Amyotrophic lateral sclerosis is a distal axonopathy: evidence in mice and man. Exp Neurol 2004;185:232–240. [PubMed: 14736504]

Fox MA, Sanes JR, Borza DB, Eswarakumar VP, Fassler R, Hudson BG, John SW, Ninomiya Y, Pedchenko V, Pfaff SL, et al. Distinct target-derived signals organize formation, maturation, and maintenance of motor nerve terminals. Cell 2007;129:179–193. [PubMed: 17418794]

Gustafsson MG. Surpassing the lateral resolution limit by a factor of two using structured illumination microscopy. J Microsc 2000;198:82–87. [PubMed: 10810003]

Gustafsson MG, Shao L, Carlton PM, Wang CJR, Golubovskaya IN, Cande WZ, Agard DA, Sedat JW. Three-dimensional Resolution Doubling in Widefield Fluorescence Micrsocopy by Structured Illumination. Biophysical Journal. 2008in press

Hortsch M, Paisley KL, Tian MZ, Qian M, Bouley M, Chandler R. The axonal localization of large Drosophila ankyrin2 protein isoforms is essential for neuronal functionality. Mol Cell Neurosci 2002;20:43–55. [PubMed: 12056839]

Jenkins SM, Bennett V. Ankyrin-G coordinates assembly of the spectrin-based membrane skeleton, voltage-gated sodium channels, and L1 CAMs at Purkinje neuron initial segments. J Cell Biol 2001;155:739–746. [PubMed: 11724816]

Jenkins SM, Bennett V. Developing nodes of Ranvier are defined by ankyrin-G clustering and are independent of paranodal axoglial adhesion. Proc Natl Acad Sci U S A 2002;99:2303–2308. [PubMed: 11842202]

Kittel RJ, Wichmann C, Rasse TM, Fouquet W, Schmidt M, Schmid A, Wagh DA, Pawlu C, Kellner RR, Willig KI, et al. Bruchpilot promotes active zone assembly, Ca2+ channel clustering, and vesicle release. Science 2006;312:1051–1054. [PubMed: 16614170]

Kordeli E, Lambert S, Bennett V, Ankyrin G. A new ankyrin gene with neural-specific isoforms localized at the axonal initial segment and node of Ranvier. J Biol Chem 1995;270:2352–2359. [PubMed: 7836469]

Kunimoto M. A neuron-specific isoform of brain ankyrin, 440-kD ankyrinB, is targeted to the axons of rat cerebellar neurons. J Cell Biol 1995;131:1821–1829. [PubMed: 8557748]

Lee YS, Carthew RW. Making a better RNAi vector for Drosophila: use of intron spacers. Methods 2003;30:322–329. [PubMed: 12828946]

Liu SC, Derick LH, Palek J. Visualization of the hexagonal lattice in the erythrocyte membrane skeleton. J Cell Biol 1987;104:527–536. [PubMed: 2434513]

Luo L, O'Leary DD. Axon retraction and degeneration in development and disease. Annu Rev Neurosci 2005;28:127–156. [PubMed: 16022592]

Marie B, Sweeney ST, Poskanzer KE, Roos J, Kelly RB, Davis GW. Dap160/intersectin scaffolds the periactive zone to achieve high-fidelity endocytosis and normal synaptic growth. Neuron 2004;43:207–219. [PubMed: 15260957]

Mi W, Beirowski B, Gillingwater TH, Adalbert R, Wagner D, Grumme D, Osaka H, Conforti L, Arnhold S, Addicks K, et al. The slow Wallerian degeneration gene, WldS, inhibits axonal spheroid pathology in gracile axonal dystrophy mice. Brain 2005;128:405–416. [PubMed: 15644421]

Pan Z, Kao T, Horvath Z, Lemos J, Sul JY, Cranstoun SD, Bennett V, Scherer SS, Cooper EC. A common ankyrin-G-based mechanism retains KCNQ and NaV channels at electrically active domains of the axon. J Neurosci 2006;26:2599–2613. [PubMed: 16525039]

Pielage J, Fetter RD, Davis GW. Presynaptic spectrin is essential for synapse stabilization. Curr Biol 2005;15:918–928. [PubMed: 15916948]

Pielage J, Fetter RD, Davis GW. A postsynaptic Spectrin scaffold defines active zone size, spacing, and efficacy at the Drosophila neuromuscular junction. J Cell Biol 2006;175:491–503. [PubMed: 17088429]

Pun S, Santos AF, Saxena S, Xu L, Caroni P. Selective vulnerability and pruning of phasic motoneuron axons in motoneuron disease alleviated by CNTF. Nat Neurosci 2006;9:408–419. [PubMed: 16474388]

Rasse TM, Fouquet W, Schmid A, Kittel RJ, Mertel S, Sigrist CB, Schmidt M, Guzman A, Merino C, Qin G, et al. Glutamate receptor dynamics organizing synapse formation in vivo. Nat Neurosci 2005;8:898–905. [PubMed: 16136672]

Roos J, Hummel T, Ng N, Klambt C, Davis GW. Drosophila Futsch regulates synaptic microtubule organization and is necessary for synaptic growth. Neuron 2000;26:371–382. [PubMed: 10839356]

Saxena S, Caroni P. Mechanisms of axon degeneration: from development to disease. Prog Neurobiol 2007;83:174–191. [PubMed: 17822833]

Schuster CM, Davis GW, Fetter RD, Goodman CS. Genetic dissection of structural and functional components of synaptic plasticity. I. Fasciclin II controls synaptic stabilization and growth. Neuron 1996;17:641–654. [PubMed: 8893022]

Scotland P, Zhou D, Benveniste H, Bennett V. Nervous system defects of AnkyrinB (−/−) mice suggest functional overlap between the cell adhesion molecule L1 and 440-kD AnkyrinB in premyelinated axons. J Cell Biol 1998;143:1305–1315. [PubMed: 9832558]

Sweeney ST, Davis GW. Unrestricted synaptic growth in spinster-a late endosomal protein implicated in TGF-beta-mediated synaptic growth regulation. Neuron 2002;36:403–416. [PubMed: 12408844]

Wagh DA, Rasse TM, Asan E, Hofbauer A, Schwenkert I, Durrbeck H, Buchner S, Dabauvalle MC, Schmidt M, Qin G, et al. Bruchpilot, a protein with homology to ELKS/CAST, is required for structural integrity and function of synaptic active zones in Drosophila. Neuron 2006;49:833–844. [PubMed: 16543132]

Wang M, Wu Y, Culver DG, Glass JD. The gene for slow Wallerian degeneration (Wld(s)) is also protective against vincristine neuropathy. Neurobiol Dis 2001;8:155–161. [PubMed: 11162249]

Watts RJ, Hoopfer ED, Luo L. Axon pruning during Drosophila metamorphosis: evidence for local degeneration and requirement of the ubiquitin-proteasome system. Neuron 2003;38:871–885. [PubMed: 12818174]

Yamamoto M, Ueda R, Takahashi K, Saigo K, Uemura T. Control of axonal sprouting and dendrite branching by the Nrg-Ank complex at the neuron-glia interface. Curr Biol 2006;16:1678–1683. [PubMed: 16920632]

Yang Y, Ogawa Y, Hedstrom KL, Rasband MN. betaIV spectrin is recruited to axon initial segments and nodes of Ranvier by ankyrinG. J Cell Biol 2007;176:509–519. [PubMed: 17283186]

Zhai Q, Wang J, Kim A, Liu Q, Watts R, Hoopfer E, Mitchison T, Luo L, He Z. Involvement of the ubiquitin-proteasome system in the early stages of wallerian degeneration. Neuron 2003;39:217–225. [PubMed: 12873380]

Zhang X, Bennett V. Restriction of 480/270-kD ankyrin G to axon proximal segments requires multiple ankyrin G-specific domains. J Cell Biol 1998;142:1571–1581. [PubMed: 9744885]

Zhou D, Lambert S, Malen PL, Carpenter S, Boland LM, Bennett V. AnkyrinG is required for clustering of voltage-gated Na channels at axon initial segments and for normal action potential firing. J Cell Biol 1998;143:1295–1304. [PubMed: 9832557]

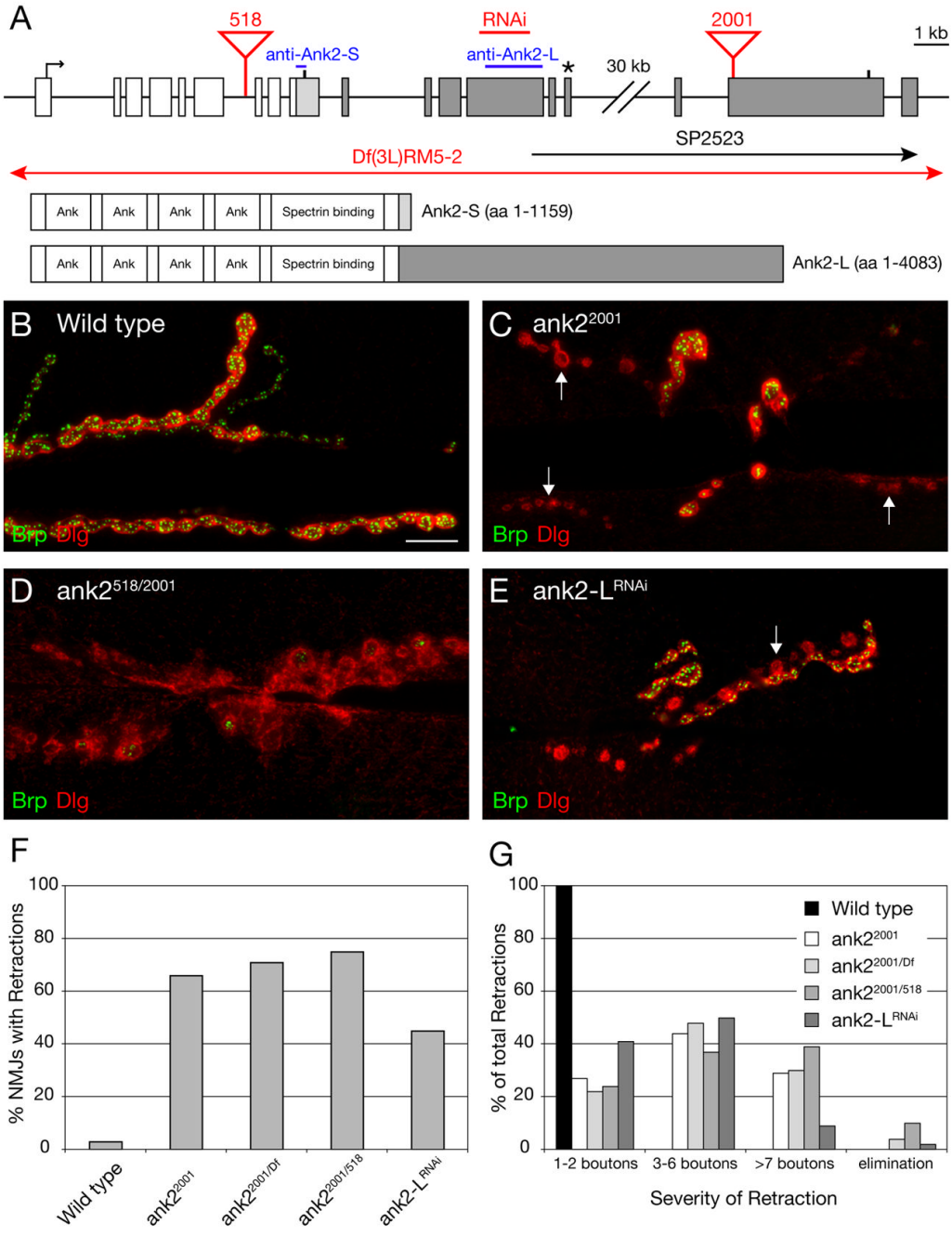

Figure 1. A novel, giant Ankyrin2 is required for synapse stability

A) Schematic of the *ank2* gene locus. The exons and protein structure of the 2 major isoforms of *ank2* are indicated. Common exons and protein sequence are denoted in white, Ank2-S specific sequences (33 aa) in light gray and Ank2-L specific sequences in dark gray. The position of the stop codons is indicated by a vertical bar. The asterisk demarcates the position of the stop codon of previously described long isoforms of *ank2* (Ank2b–e) (Hortsch et al., 2002). The position of the predicted gene *SP2523* is indicated. The position of the transposon insertion mutations and the sequence region targeted by the RNAi construct are marked in red. The regions used to generate the isoform-specific antibodies (Hortsch et al., 2002) are indicated in blue. **B–E)** NMJs at muscles 6/7 stained with the presynaptic active zone marker anti-Brp

(green) and the postsynaptic marker anti-Dlg (red). **B**) A wild type NMJ with perfect apposition between the pre- and postsynaptic markers. **C**) A homozygous mutant *ank2*^{2001} NMJ. At multiple regions within the NMJ, organized postsynaptic Dlg staining is no longer opposed by the presynaptic active zone marker Brp indicating synaptic retractions (arrows). **D**) NMJ of a trans-heterozygous *ank2*^{518}/*ank2*^{2001} animal. The NMJ shows organized postsynaptic Dlg staining with very little opposing presynaptic Brp staining indicating that the presynaptic nerve terminal has almost been eliminated. **E**) NMJ of an animal expressing *ank2-L*^{RNAi} presynaptically. One branch of the synapse has retracted and shows only postsynaptic Dlg staining (arrow). **F**) Quantification of synaptic retractions in wild type and *ank2* mutant animals. 120 NMJ (muscles 6/7) of each genotype were analyzed for synaptic retractions. **G**) Quantification of the severity of synaptic retractions. The observed synaptic retractions were quantified and grouped into different classes based on the number of Dlg-positive synaptic profiles that lack the presynaptic marker. Scale bar in B–E 10 μm.

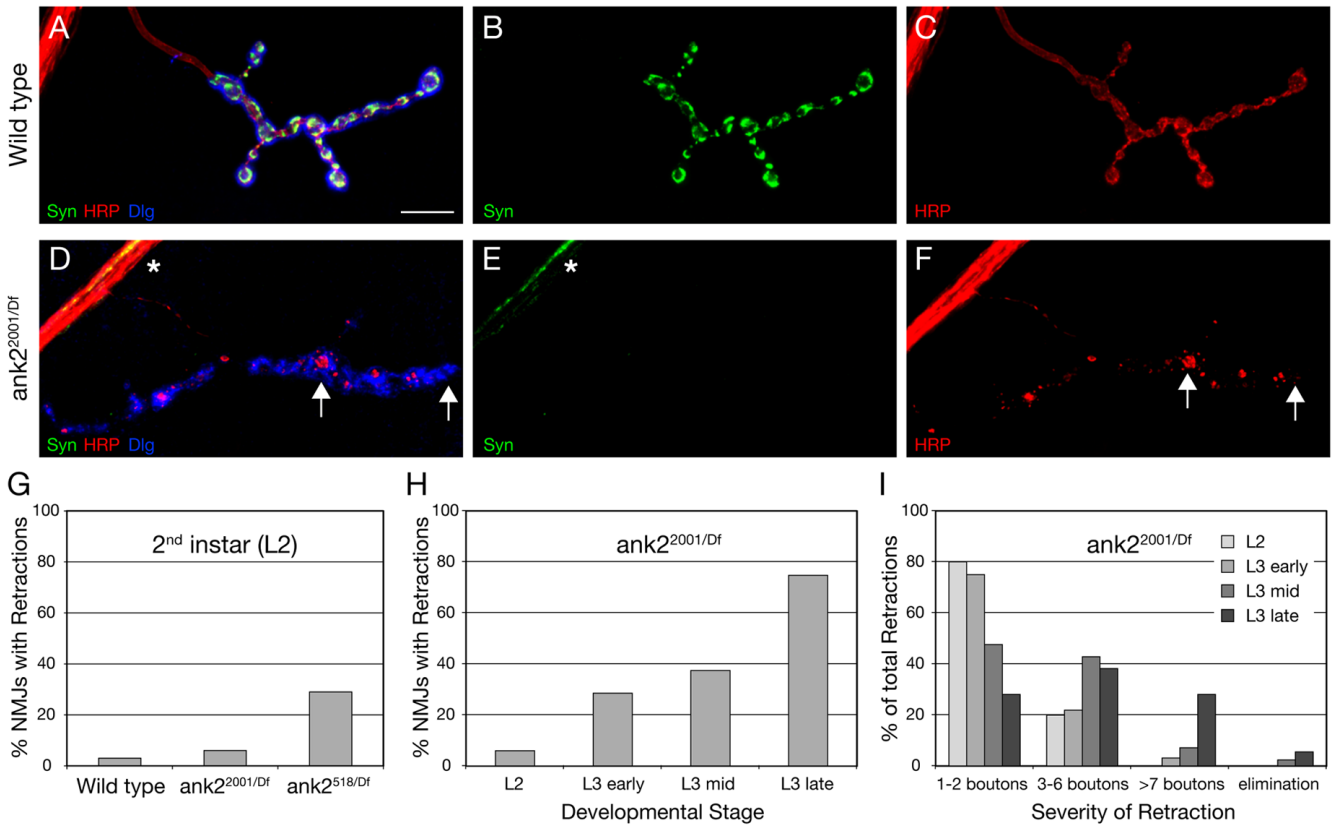

Figure 2. Analysis of synaptic retractions in *ank2* mutant animals

A–C) Wild type NMJ on muscle 4 stained for the presynaptic vesicle marker Synapsin (Syn) (green), the presynaptic membrane marker HRP (red) and postsynaptic Dlg (blue). Syn and HRP-positive presynaptic boutons are present opposite postsynaptic Dlg. **D–F)** Muscle 4 NMJ of a mutant *ank2*^{2001}*/Df* animal. While some Syn staining can be detected in the motoneuron axon (asterisk), no Syn staining is present at the NMJ opposite postsynaptic Dlg staining. The presynaptic membrane marked by HRP is no longer continuous but has fragmented and only remnants of the membrane are visible opposite postsynaptic Dlg staining (arrows). **G)** Comparison of the frequency of synaptic retractions at the second instar larval stage (L2). **H)** Developmental time course of the frequency of synaptic retraction frequency in *ank2*$^{2001/Df}$ mutant animals. **I)** Developmental time course of the severity of synaptic retraction frequency in *ank2*$^{2001/Df}$ mutant animals. Scale bar in A–F 10 μm.

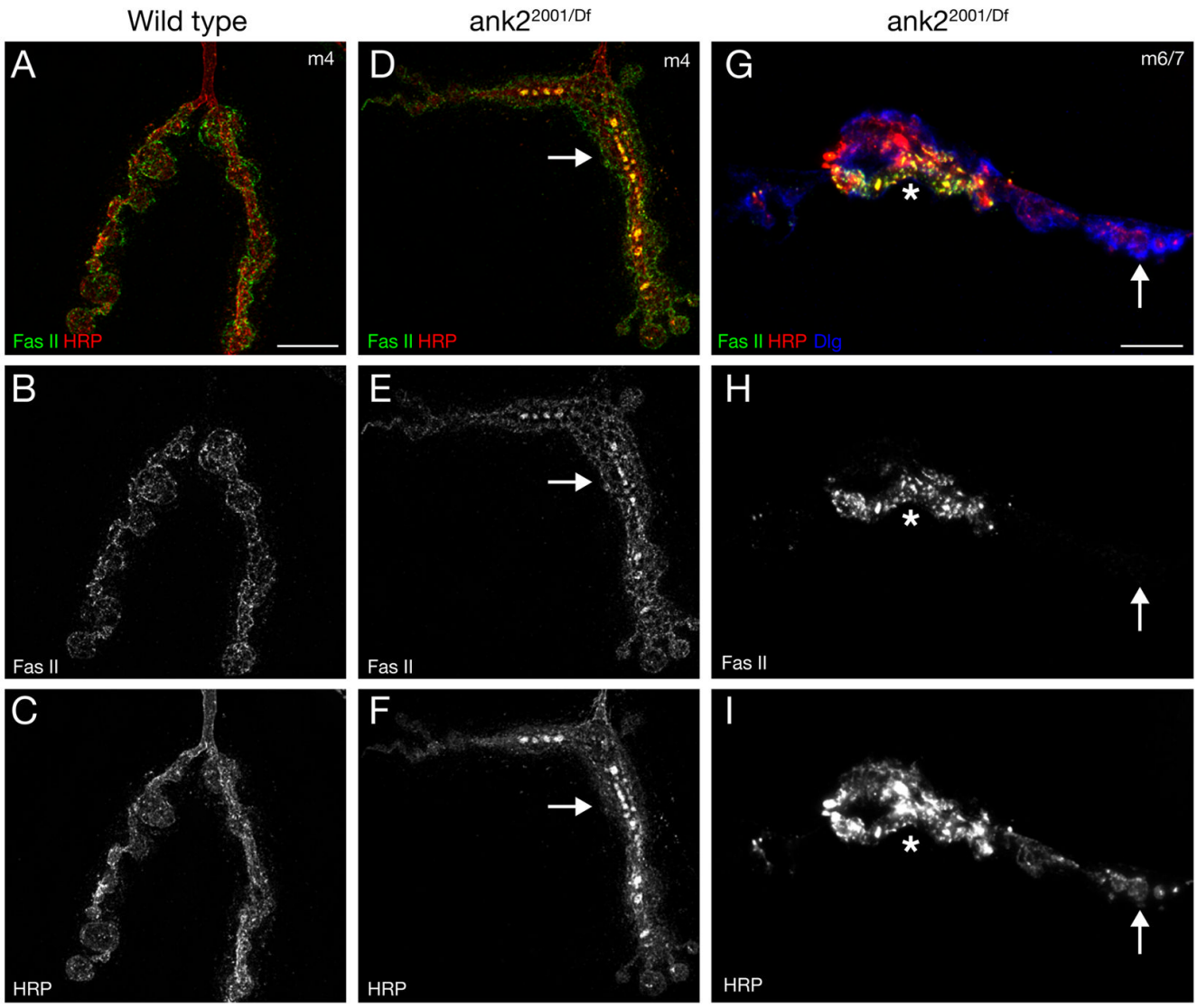

Figure 3. Ank2-L is required for the organization and stability of the synaptic cell adhesion molecule Fasciclin II

A–C) Structured-illumination image showing the distribution of the cell adhesion molecule Fasciclin II (Fas II, green) and the presynaptic membrane marker HRP (red) in wild type animals. Fas II is organized into a honeycomb-like pattern throughout synaptic boutons. **D–F**) In *ank2*$^{2001/Df\ RM5\text{-}2}$ mutant animals both the organization of the NMJ and the organization of Fas II and HRP are severely perturbed (arrows). **G–I**) We find sites within *ank2*$^{2001/Df\ RM5\text{-}2}$ mutant NMJs where Fas II levels are greatly reduced and almost absent while the membrane marker HRP is still present opposite postsynaptic Dlg (arrow). At these sites the HRP staining starts to become fragmented (arrow). Scale bar A–F 5 μm. Scale bar in G–I 10 μm.

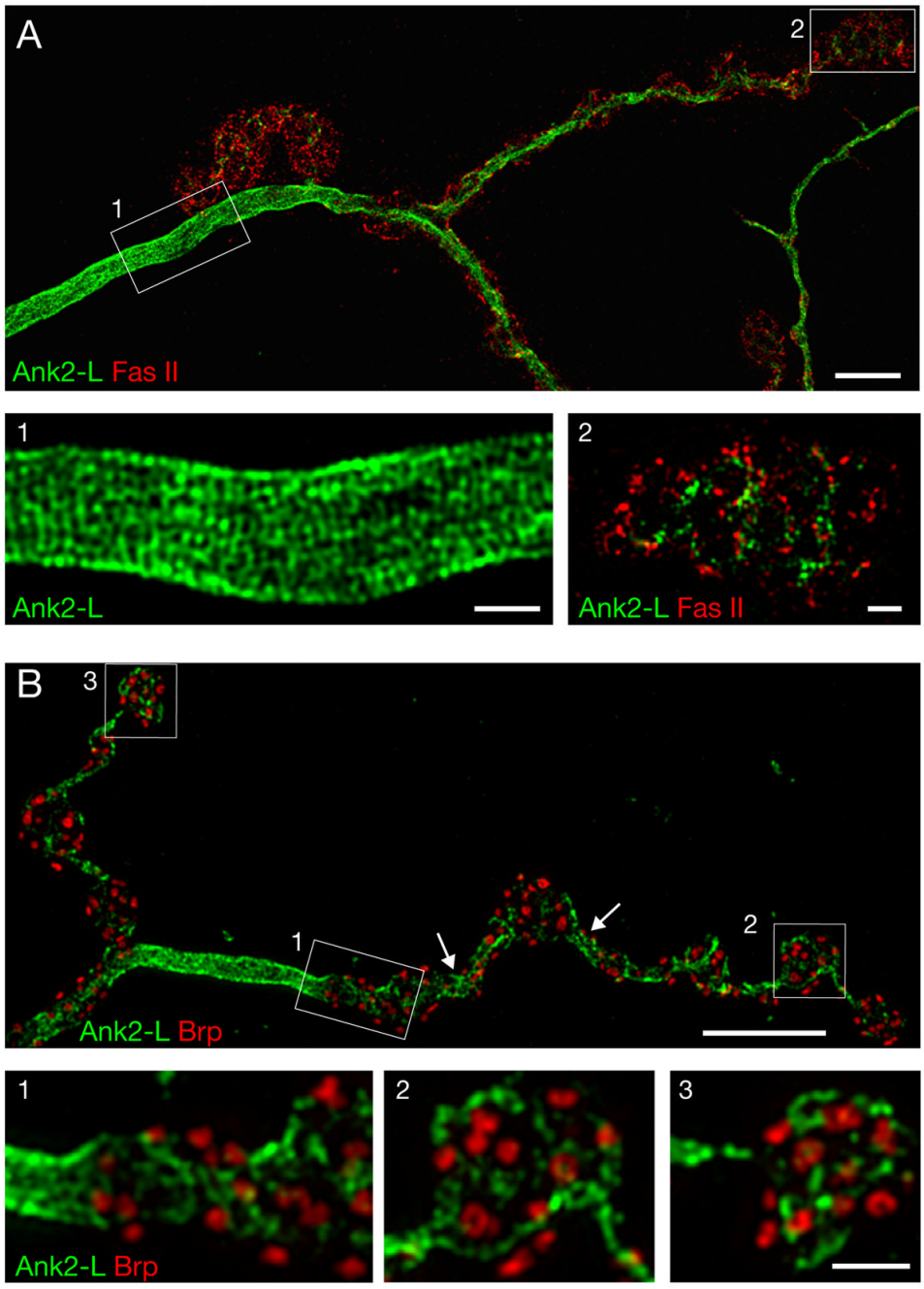

Figure 4. Structured-illumination microscopy reveals unique axonal and synaptic organization of Ank2-L

A)A wild type muscle 4 NMJ stained for Ank2-L (green) and the cell adhesion molecule Fas II (red). Ank2-L is highly organized into a repetitive lattice with a periodicity of approximately 200 nm within the motoneuron axon prior to the innervation of the muscle (inset 1). Within synaptic boutons Ank2-L is less well organized. It localizes to a membrane domain similar to that occupied by Fas II (inset 2). **B**) A wild type muscle 4 NMJ stained for Ank2-L (green) and the active zone marker Brp (red). Highly organized Ank2-L can be observed in inter-bouton regions (arrows, inset 1). Ank2-L does not co-localize with Brp and is loosely organized within synaptic boutons (insets 2, 3). Scale bar in A, B 5 μm, in insets 1 μm.

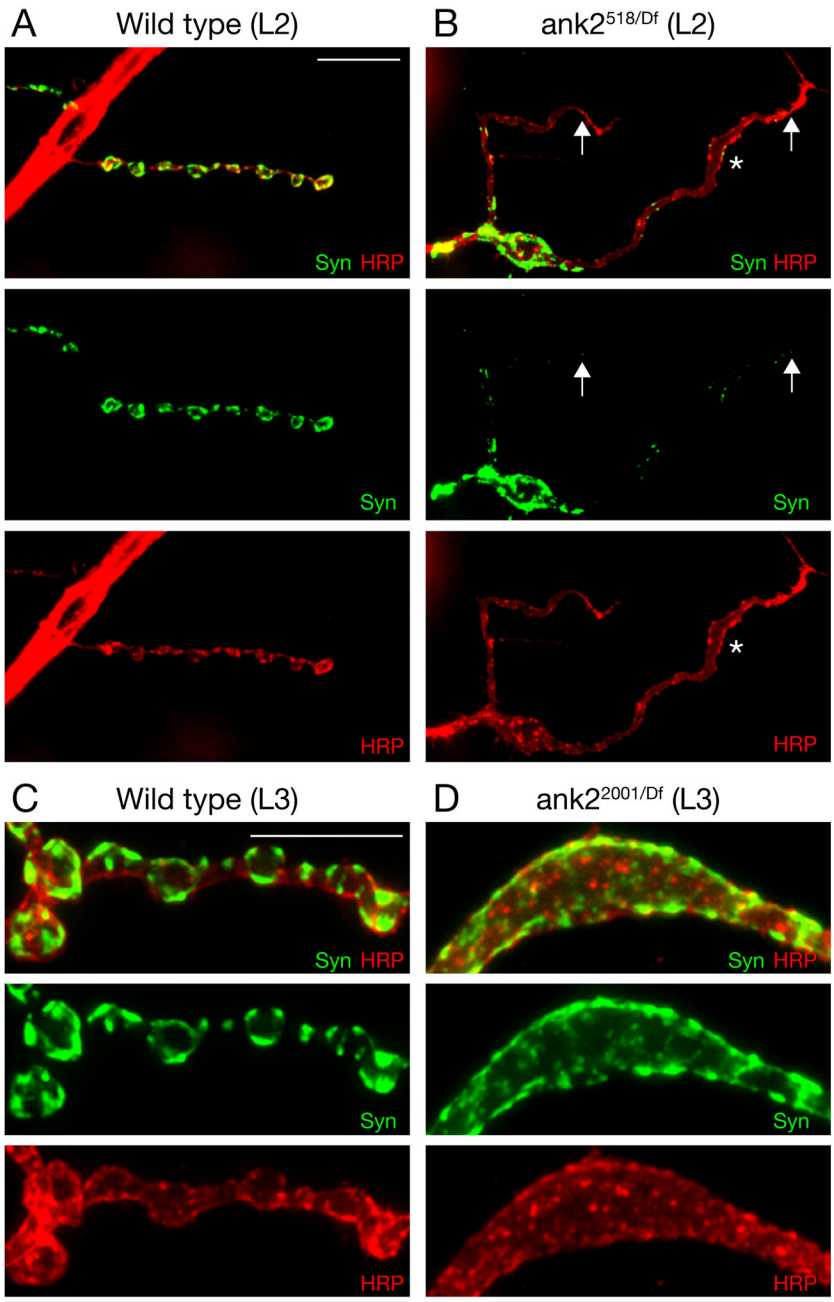

Figure 5. Ank2-L is required for normal synapse morphology and sub-synaptic organization

A-B) Second instar muscle 4 NMJ stained for the presynaptic vesicle marker Synapsin (green) and the presynaptic membrane marker HRP (red). **A**) Wild type synapses show clearly organized synaptic boutons that include distinct Synapsin-labeled domains. **B**) Synapse organization is severely perturbed in *ank2*$^{518/Df}$ mutant animals including the loss narrow-diameter inter-bouton regions. The NMJ appears as a ribbon of uniform width (asterisk). Syn is less abundant at distal parts of the NMJ (arrows) **C**) At third instar wild type NMJ the partitioning of the presynaptic nerve terminal into a series of synaptic boutons that contain sub-domains of Syn is visible. **D**) In *ank2*$^{2001/Df\ RM5\text{-}2}$ mutant NMJs, large presynaptic membrane

compartments are observed and Syn staining is no longer evenly partitioned into distinct domains. Scale bar in A, B 10 μm; scale bar in C, D 10 μm.

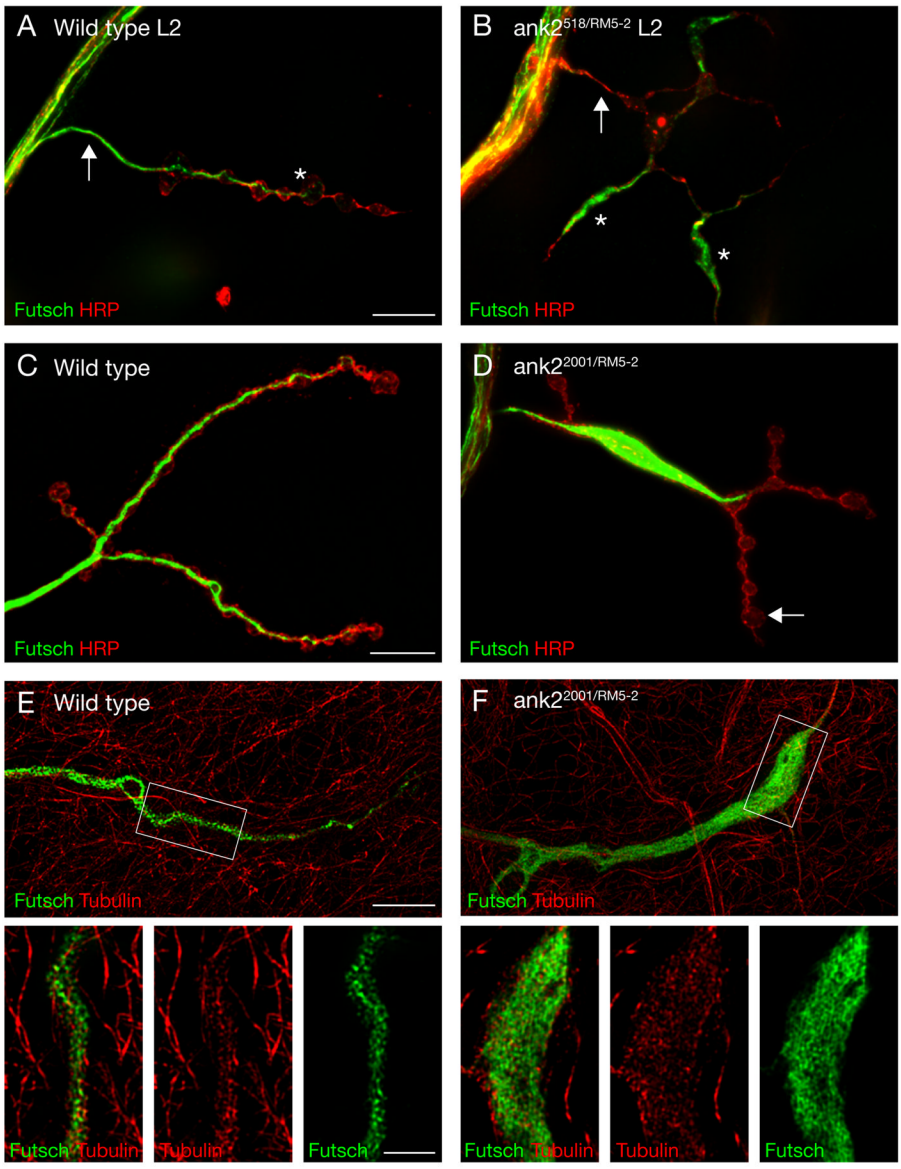

Figure 6. Ank2 is required for the organization of synaptic microtubules

A,B) Second instar muscle 4 NMJs stained for the microtubule-associated protein Futsch (green) and the presynaptic membrane marker HRP (red). **A**) A wild type synapse. The core microtubule filament extends into the terminal boutons. **B**) In *ank2*$^{518/Df\ RM5\text{-}2}$ mutant animals we observe large accumulations of Futsch in some regions of the synapse (asterisks) while Futsch is almost absent in other regions (arrow). **C, D**) Third instar muscle 4 NMJs. **C**) In wild type the core microtubule filament becomes progressively thinner as it extends into the nerve terminal. **D**) In *ank2*$^{2001/Df\ RM5\text{-}2}$ mutant animals large accumulations of Futsch are present and the core microtubule filament no longer extends into all terminal boutons (arrow). **E, F**) High-resolution structured-illumination images of Futsch (green) and microtubules (red). **E**) In wild type synapses Futsch is tightly associated with presynaptic microtubules that form a core filament. **F**) In *ank2*$^{2001/Df\ RM5\text{-}2}$ mutant animals the microtubules are no longer organized into a core filament but occupy large regions of the synapse. In the high magnifications the simultaneous disruption of Futsch and microtubule organization is clearly evident. Scale bar A, B and C, D 10 μm; scale bar in E, F 5 μm, insets 2 μm.

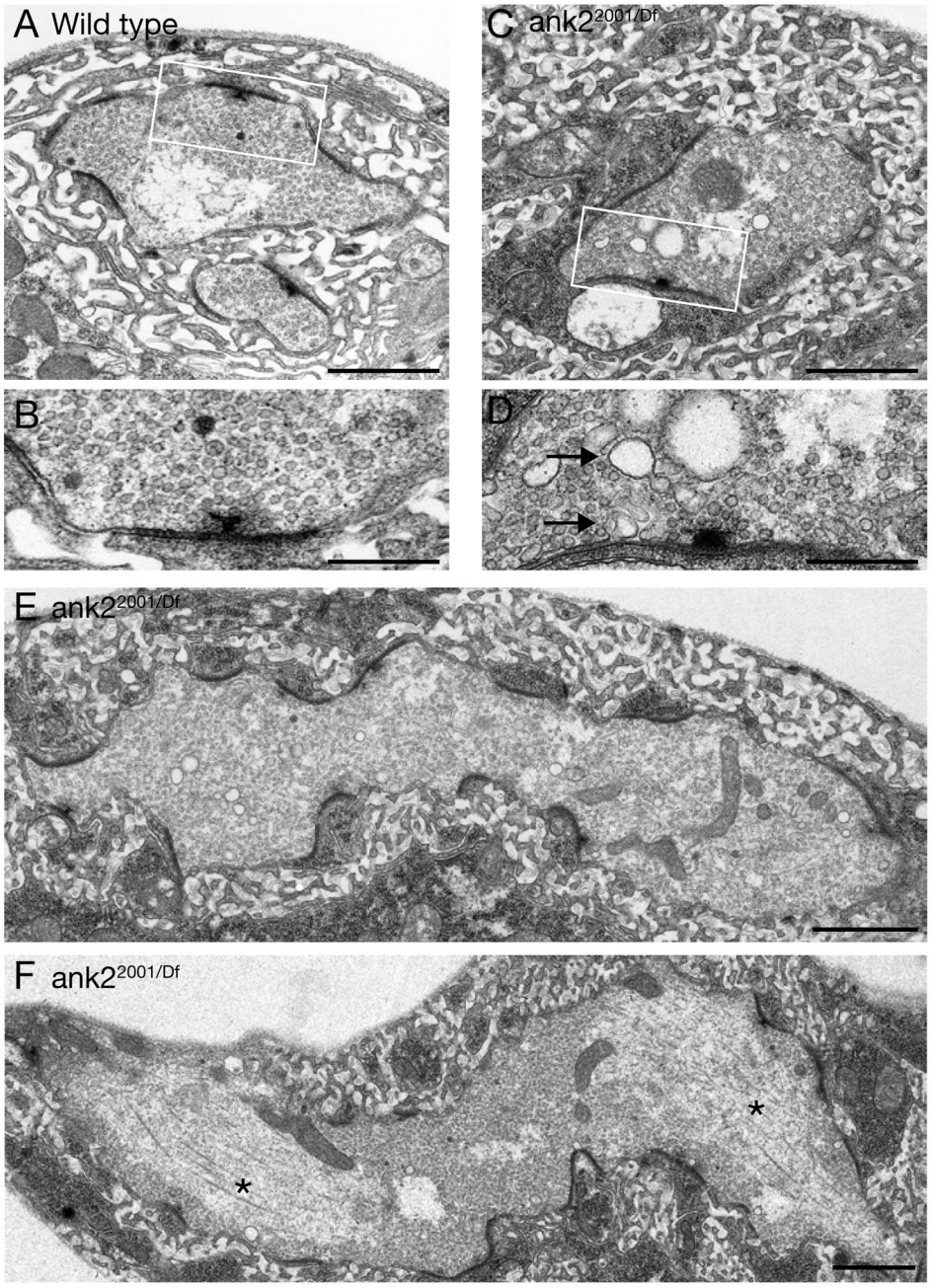

Figure 7. Ultrastructural analysis of *ank2* mutant animals

A,B) Wild type synaptic boutons within muscles 6/7 are embedded in organized postsynaptic membranes. The boxed area is shown in B at a higher resolution. Regular sized synaptic vesicles are found in the presynaptic region close to an active zone with a T-bar. **C, D**) A muscle 6/7 bouton of an *ank2*$^{2001/Df\ RM5\text{-}2}$ mutant animal shows signs of synapse degeneration. The boxed area is shown at higher magnification in D. Multiple large vesicles are visible (arrows). **E, F**) Giant synaptic boutons can be found in *ank2*$^{2001/Df\ RM5\text{-}2}$ mutant animals. The boutons are elongated laterally and multiple active zones (electron dense regions) can be detected. In addition, large vesicles are present consistent with synapse disassembly. We can observe large

accumulations of microtubules in these giant boutons (F, asterisks). Synaptic vesicles are absent from these regions. Scale bar in A, C, E, F 1 μm; scale bar in B, D 400 nm.

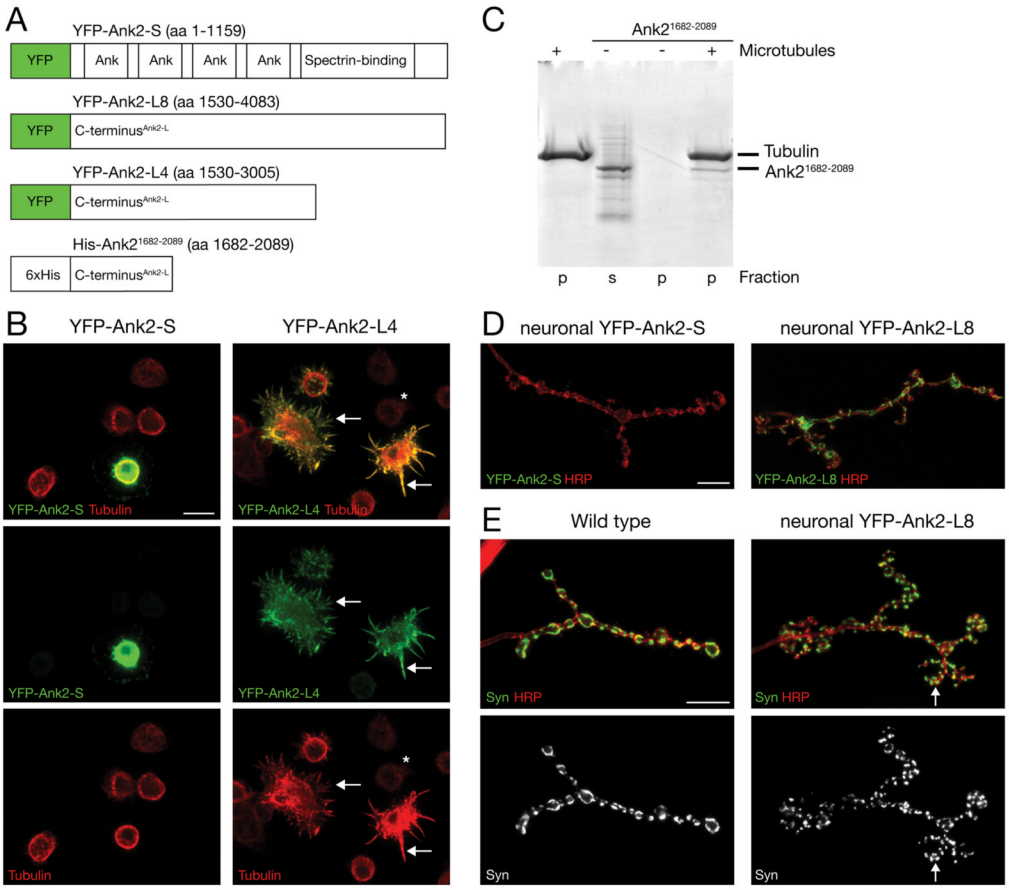

Figure 8. The C-terminal tail of Ank2-L can bind to and alter the organization of microtubules and is sufficient for the synaptic localization of Ank2-L

A) Schematic showing the different YFP/His_6-tagged *ank2* constructs. **B**) Expression of YFP-Ank2-S and YFP-Ank2-L4 in Drosophila S2 cells. The presence of YFP-Ank2-L4 severely alters the abundance and organization of microtubules. Compared to untransfected cells (asterisk) we observe an increase in Tubulin levels and a severe reorganization of microtubules (arrows). YFP-Ank2-L4 co-localizes with the altered microtubules that appear bundled and form spike like processes (right panels). In contrast, the presence of YFP-Ank2-S does not significantly alter abundance or distribution of microtubules (left panels). **C**) Microtubule pelleting assay. The C-terminal fragment of Ank2 ($Ank2^{1682–2089}$) can be detected in the pellet fraction in the presence of taxol-stabilized microtubules (right lane) indicating microtubule binding. In the absence of microtubules $Ank2^{1682–2089}$ can only be detected in the supernatant. **D**) Neuronal over-expression of YFP-Ank2-S (left) and YFP-Ank2-L8 (right) in motoneurons in wild type animals. Only YFP-Ank2-L8 is efficiently trafficked to the presynaptic nerve terminal. **E**) Over-expression of high levels of presynaptic YFP-Ank2-L8 results in a severe perturbation of NMJ development. Compared to wild type synapses (left panels) multiple small satellite boutons form that branch of the main shaft. The satellite boutons can be identified by the presynaptic membrane marker HRP or the presynaptic vesicle marker Synapsin. Sub-domains of Synapsin can be detected in small satellite boutons (arrow). Scale bar in B, D, E 10 μm.